Decoupling Control Applied to the Smart Grid Power Dispatching Problem

Salim Nebili
Department of Physics, Laboratory of Electrical and Energetic Systems, Faculty of Sciences of Tunis, University of Tunis El Manar, Tunis, Tunisia
salim.nebili@tunisietelecom.tn

Ibrahim Benabdallah
Department of Physics, Laboratory of Electrical and Energetic Systems, Faculty of Sciences of Tunis, University of Tunis El Manar, Tunis, Tunisia
ibrahim.benabdallah@gmail.com

Adnen Cherif
Department of Physics, Laboratory of Electrical and Energetic Systems, Faculty of Sciences of Tunis, University of Tunis El Manar, Tunis, Tunisia
adnen2fr@yahoo.fr

Received: 15 May 2022 | Revised: 9 June 2022 | Accepted: 13 June 2022

Abstract-This paper presents controller designs of the decoupling issue dedicated to renewable decentralized generators or new generation grids known as smart grids. The control methods were based on a three-phase voltage source grid representation that integrated wind and photovoltaic generators. The utilized decoupling strategies (Boksenbom and Hood, Zilkind and Luyben, and inverted decoupling) allowed the optimization of energy transfers and costs through the routing grid distribution path. Simulations were conducted in Matlab/Simulink. The trustworthiness of the multivariable control system design in addition to the tuning method was established using three test batches, totally decoupled and stable from input dependencies.

Keywords-decoupling; smart grid; demand-response; power dispatching; controller design

I. INTRODUCTION

Methods presenting only one output controlled by a single deployed variable are classified as Single-Input Single-Output (SISO) systems. Several processes do not imitate such a simple control shape. Each unit operation needs to control no less than two variables, and consequently, there are frequently at least two control loops to deal with. Systems that involve more than one control loop are known as Multi-Input Multi-Output (MIMO) or multivariable systems. The electrical smart grid is essentially a massive MIMO system. Due to the interactions of the flow power offer and demand, it is not easy to design a robust controller for each path autonomously to lead an input x to an output y without affecting any other output. Many studies have focused on several loop control structures to diminish these interactions.

Decoupling methods are mostly used in industrial processes but are still applicable for many electrical system parameter-decoupling purposes. A simplified, ideal, and inverted decoupling comparative study was presented in [1], which was the base for many classic studies. Three decoupling methods were considered to deal with stability, robustness, and implementation aspects, while the complexity of the decoupler elements depended on the overall system size. An improvement of the two inverted decoupling methods was presented in [2] for the case of a stable linear multivariable class of processes, through no minimum-phase zeros and multiple time delays. As some multivariable processes were still unable to be decoupled due to stability issues, alternative decoupling with a unity feedback structure was suggested. The PI/PID was designed using internal model control to decouple the processes. In the case of multiplicative input uncertainty, the low bounds of the control parameters were intended to guarantee the robust stability of the system. As the disturbances influence the way of the control synthesis of a MIMO system based on ideal decouplers and a PID regulator, single controller performance and robustness from the closed-loop could be prolonged to all loop systems [3]. An improved decoupling approach allowed more flexibility in the choice of transfer functions of the decoupled apparent process for general $n \times n$ processes, where the decoupler elements' complexity appeared independent of the system's size [4]. A decoupling internal model controller design method was proposed in [5] for industrial MIMO time-delay systems, based on a controlled model adjoint matrix. A decoupling compensator and an internal model controller, Butterworth low-pass filter, were designed for decoupling the generalized controlled object. The last filter aimed to improve the disturbance rejection aptitude. In [6], a method of finding the forced oscillation source was proposed. The relation between the observable outputs and the mechanical power problems in a unit was decoupled by sensibly designing a Luenberger observer using an aging structure task. A MIMO control system with multiple time delays and a model predictive control was presented in [7], describing a method to design MIMO filtered Smith predictors for $n \times n$ processes through multiple time delays based on the decentralized direct decoupling structure. This allowed simple tuning of the primary controller, making simpler the problem toward multiple single loops, if realizable, and it could also be used to eliminate the interactions among process variables.

The decoupling method is also applicable to electrical grid, microgrid, and smart grid annexed domains facing new intermittent and highly variable system challenges and expectations [8-17]. Modeling approaches were proposed in [8] using analytical tools for control design purposes of step-up grid-connected PV systems, such as voltage source

Corresponding author: Salim Nebili

representation of the bulk capacitor interacting with the grid-connected inverter and considering the inverter of a double-stage PV system as a Norton equivalent. Furthermore, both ideal and real DC/DC converter models for the PV module were presented through four mathematical models, stated in state-space representation. A decoupled inverter connected to a grid was exposed in [9], using dynamic online grid impedance measurements in a micro grid application. The controller was implemented in a synchronous reference frame and PI controllers were used, while mutual coupling was introduced between the *d* and *q* control loops. The transformation into a synchronous reference was accurately decoupled using the dynamically measured grid impedance and feedforward control. Decoupling permits autonomous control of active and reactive powers following changes, and online real impedance measurement was proposed to make the decoupling more precise. In [10], a multivariable-droop synchronous current converter decoupling control strategy was proposed for the current management of weak grid/micro grid applications, offering a traditional forward design method that employs the loop determining technique. The controller mixes current regulation, management, and limitations that apply to weak and micro grids. The multivariable synchronous current converter allowed larger decoupling of d- and q-axis currents in weak and/or resistive grids, anywhere these control variables are highly coupled due to the converter's large load-angle operation.

In [11], the evolution allocation for the decoupling of the electrical network was studied using pure channel component transform, addressing issues such as robustness. Difficulties were efficiently overcome using singular values instead of proper decomposition. An algorithm was developed to show how the adopted transformation can be used for voltage stability analysis. In [12], a distributed generator strategy control was investigated to assist a conventional local grid by decoupling phase sequences, frequency domain unbalances, and harmonic compensation for grid-connected inverters through unbalanced loads. This strategy was considered sequential-asymmetric for unbalanced and harmonic voltage correction. Moreover, a Norton equivalent model in frequency-domain was used. This study showed that following a frequency-domain decoupled method, the fundamental positive, harmonic symmetrical, fundamental zero, and negative sequence components can be regulated independently.

In [13], a virtual synchronous generator control method was proposed for extensive renewable energies connected to a grid. A power decoupling control method based on linear active disturbance rejection control was developed to eliminate output power deviation. Using the coupling term estimates and disturbances from an extended state observer, the aforesaid matter triggered by power coupling can be lessened. Furthermore, the stability of the controller was analyzed. In [14], essential limitations were defined for the islanded mode of operation of micro grids which cannot be absorbed by conventional FP methods. Therefore, updates were designed for conservative approaches by including network frequency as a variable and avoiding the network soft bus. These particular aspects of the Newton-Raphson method modified the designs of the Jacobean matrix. Extended power factor equations were decoupled by reformulating the Jacobean matrix based on the fact that lines are mostly resistive. Furthermore, two convergence improvement methods were also incorporated. Dual-buck inverters were examined in [15], reassessing volume, system weight, and power density of dual-buck single-phase grid-tied PV inverters. A new active power decoupling buffer and grid-tied photovoltaic inverter integration with single-inductor dual buck topology were proposed, using a single-loop direct input current ripple control method. Several concerns arise in the case of pulse width modulation using a high-voltage current source converter based on fully controlled devices, such as high switching losses, large DC voltage fluctuations, and thin power operation range [16]. To resolve these difficulties, a current source converter-based HVDC was proposed using fundamental frequency modulation presenting the topology, an independent control strategy, and a mathematical model. A synchronized control strategy was proposed to decouple active and reactive powers with an outer and inner current controller loop to lead to lower DC voltage fluctuations, lower switching losses, and a broader power operation range.

This study investigated a Two-Input Two-Output (TITO) grid system, as a MIMO system could be devised into several TITO subsystems. The main goal was to employ decoupling methods for grid part energy aggregation, aiming to decouple demand response paths based on statue and output feedback control methods.

II. CONTROLLER DESIGN AND METHODS

The control strategy of the phase grid-connected PV, wind, and storage system inverter is presented in Figure 1. The elements were taken from [17-24].

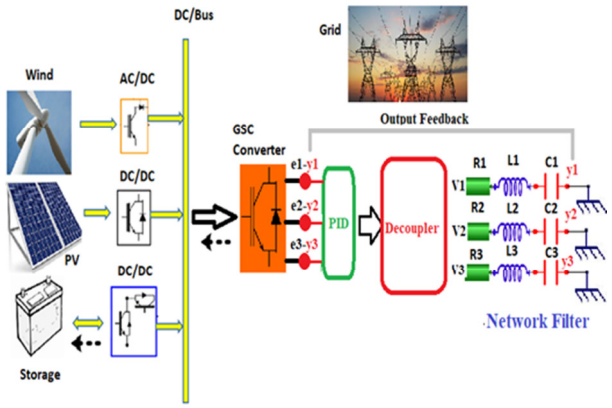

Fig. 1. Overall grid-connected system design.

The system can be described in the state representation by:

$$\begin{cases} \dot{X} = AX + BU \\ Y = CX + DU \end{cases} \quad (1)$$

where *A* is the characteristic matrix, *B* is the order matrix, *C* is the output matrix, and *D* is the coupling matrix. A control law was defined by the output feedback as:

$$e = V - K.y \quad (2)$$

where V is the new entries vector of the dimension ($m.1$), K is the matrix of dimension ($m.l$), m is the number of outputs, l is the number of entries, y is the output vector, and e is the input vector. K is calculated by solving:

$$|\lambda I - BKC| = 0 \quad (3)$$

The governing equations of the network filter defined in Figure 1 are:

$$\begin{cases} \frac{L_1 dI_1}{dt} + R_1 I_1 + V_1 = y_1 \\ \frac{L_2 dI_2}{dt} + R_2 I_2 + V_2 = y_2 \\ \frac{L_3 dI_3}{dt} + R_3 I_3 + V_3 = y_3 \end{cases} \quad (4)$$

The fundamental principles of simplification of the equations of states, such as the Park model, can be used to either substitute or eliminate the effect of one or several equations, to implement and succeed in the decoupling methods by delimitating the effects of inputs on outputs. The relative Park equation model from the overall grid-connected system design is given by:

$$\begin{cases} \frac{L_d dI_d}{dt} + R_d I_d + V_d = y_d \\ \frac{L_q dI_q}{dt} + R_q I_q + V_q = y_q \end{cases} \quad (5)$$

Input and output voltages are linked by values belonging to $\mathbb{R}$:

$$\begin{cases} V_d = \lambda_d y_d + \lambda_q y_q \\ V_q = \beta_d y_d + \beta_q y_q \end{cases} \quad (6)$$

Using (5):

$$\begin{cases} \frac{L_d dI_d}{dt} = -R_d I_d - V_d + y_d \\ \frac{L_q dI_q}{dt} = -R_q I_q - V_q + y_q \end{cases} \quad (7)$$

Substituting (6) in (7) gives:

$$\begin{aligned} \frac{L_d dI_d}{dt} &= -R_d I_d - (\lambda_d y_d + \lambda_q y_q) + y_d \\ \frac{L_q dI_q}{dt} &= -R_q I_q - (\beta_d y_d + \beta_q y_q) + y_q \end{aligned} \quad (8)$$

$$A = \begin{bmatrix} \frac{-R_d}{L_d} & 0 \\ 0 & \frac{-R_q}{L_q} \end{bmatrix}, B = \begin{bmatrix} \frac{(1-\lambda_d)}{L_d} & \frac{-\lambda_q}{L_d} \\ \frac{-\beta_d}{L_q} & \frac{(1-\beta_q)}{L_q} \end{bmatrix} \quad (9)$$

$$C = \begin{bmatrix} 1 & 0 \\ 0 & 1 \end{bmatrix}, D = \begin{bmatrix} 0 & 0 \\ 0 & 0 \end{bmatrix}$$

The transfer function matrix $G(s)$ can be easily obtained from the state representation using:

$$G(s) = C(sI - A)^{-1}B + D \quad (10)$$

In the general case, the matrix D is null and the calculation of $G(p)$ is simplified as:

$$G(s) = C(sI - A)^{-1}B \quad (11)$$

$$G(s) = \begin{bmatrix} G_{11} & G_{12} \\ G_{21} & G_{22} \end{bmatrix} \quad (12)$$

The used units are $L_1 = L_2 = 16.58.10^{-3}$H, and $r_1 = r_2 = 0.98\Omega$. The transfer matrix is obtained from the A, B, and C matrices:

$$G(s) = \begin{bmatrix} \frac{0.096}{100s+0.96} & \frac{0.096}{100s+0.96} \\ \frac{-0.024}{100s+1.92} & \frac{0.072}{100s+1.92} \end{bmatrix} \quad (13)$$

III. SIMULATION RESULTS

The grid inputs are two photovoltaic conversion chain outputs by two different steps:

A. *Without Decoupling*

After obtaining the coupled system block diagram and the transfer matrix $G(p)$ elements, the wiring was designed in Matlab/Simulink to visualize the evolution of its outputs as a function of time. The simultaneous excitation of e1 and e2 inputs is shown in Figure 2.

$$\begin{cases} y_1 = u_1 G_{11} + u_2 G_{12} \\ y_2 = u_1 G_{21} + u_2 G_{22} \end{cases} \quad (14)$$

$$y = Gu \quad (15)$$

with:

$$y = [y_1, y_2]^T, u = [u_1, u_2]^T, G = \begin{bmatrix} G_{11} & G_{12} \\ G_{21} & G_{22} \end{bmatrix}$$

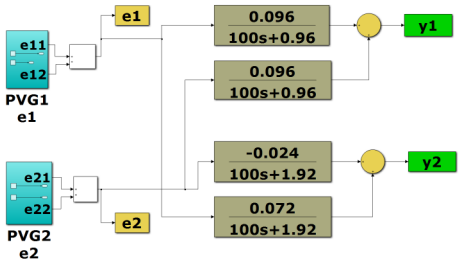

Fig. 2. Coupled system block Simulink diagram.

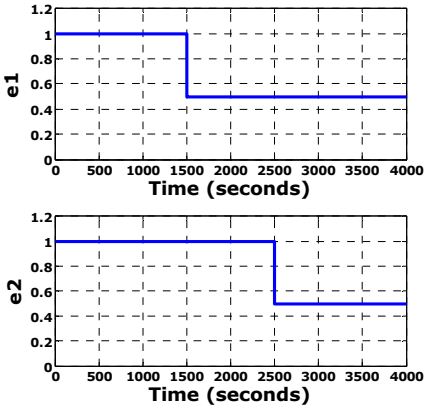

Fig. 3. Grid inputs.

At t_0=0s, a unit step is performed at each system input. Then the amplitude of e1 is reduced to 0.5 at t=1500s without modifying the second input. After that, at t=2500s, the second input e2 decreases to 0.5, without modifying the first input e1. Figure 4 shows the evolution of each output y1 and y2.

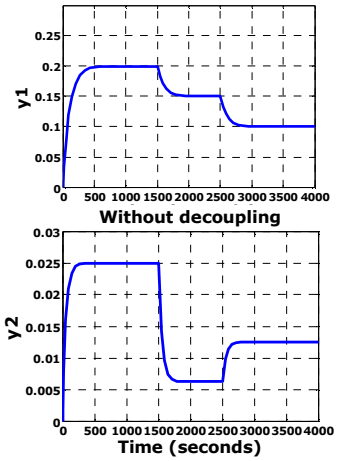

Fig. 4. Grid outputs without decoupling

The evolution of outputs of the coupled system shows that the change in the first input could vary and affect the second output. The following subsection introduces some decoupling methods to obtain an overall system made of TITO subsystems varying in parallel to Figure 5. In particular, the input e1 should only affect the first output y1, and the input e2 should only affect y2. The chosen methods were Boksenbom and Hood [2, 10], Zalkind and Luyben [2], and a method based on inverted decoupling [2, 4].

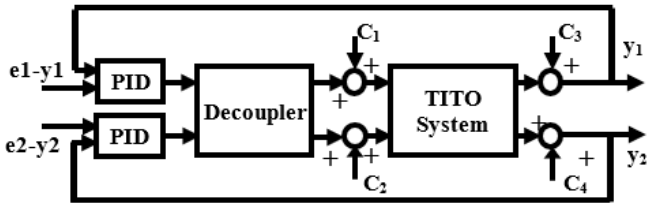

Fig. 5. The TITO overall system.

B. Decoupling Using Boksenbom and Hood Method

Using (12), the decoupling matrix G_c^* can be given by:

$$G_c^* = \begin{bmatrix} G_{c,11}^* & G_{c,12}^* \\ G_{c,21}^* & G_{c,22}^* \end{bmatrix} \text{....(16)}$$

Reference signals are shown by w=[w_1, w_2]:

$$Gu = y\,, u = G_c^*[w-y]G_c^*[w-y] = y \quad (17)$$

$$y = [I + GG_c^*]^{-1}GG_c^*w \quad (18)$$

$$X = [I + GG_c^*]^{-1}GG_c^* = diag[x_1, x_2] \quad (19)$$

X is a diagonal matrix:

$$GG_c^* = \begin{bmatrix} G_{11} & G_{12} \\ G_{21} & G_{22} \end{bmatrix} \begin{bmatrix} G_{c,11}^* & G_{c,12}^* \\ G_{c,21}^* & G_{c,22}^* \end{bmatrix} \begin{bmatrix} q_1 & 0 \\ 0 & q_2 \end{bmatrix} \quad (20)$$

$$\begin{Bmatrix} q_1 = G_{11}G_{c,11}^* + G_{12}G_{c,21}^* \\ 0 = G_{11}G_{c,12}^* + G_{12}G_{c,22}^* \\ 0 = G_{21}G_{c,11}^* + G_{22}G_{c,21}^* \\ q_2 = G_{21}G_{c,12}^* + G_{22}G_{c,22}^* \end{Bmatrix} \quad (21)$$

$$G_{c,12}^* = \frac{-G_{12}G_{c,22}^*}{G_{11}}\,,\quad G_{c,21}^* = \frac{-G_{21}G_{c,11}^*}{G_{22}} \quad (22)$$

As the decoupled matrix functions do not influence the evaluation of the diagonal matrix decoupling, according to this method principle, the PI/PID regulators must be chosen arbitrarily. The stability condition of the system has to be respected, as follows:

$$G_{c,11}^* = G_{c,22}^* = \frac{s+0.1}{s} \quad (23)$$

The Simulink transfer functions block wiring which characterizes this method are shown in Figure 6.

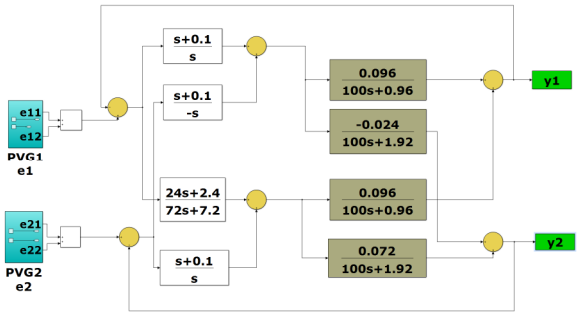

Fig. 6. Boksenbom and Hood block Simulink diagram.

The same conditions were applied in this case. At t_0=0s, a unit step was performed for e1 and e2. Then, e1 was lowered to 0.5 at t=1500s without changing e2. Next, as t=2500s, e2 declined to 0.5, without changing e1. The evolution of y1 and y2 outputs is shown in Figure 7.

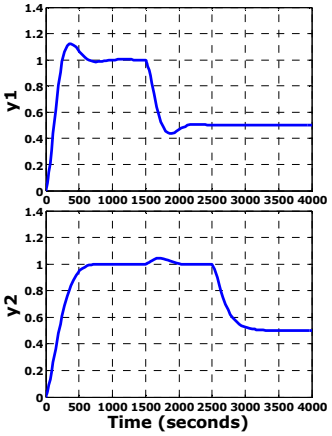

Fig. 7. Boksenbom and Hood grid outputs.

The proposed control system is perceived as having good decoupling. Due to error approximation, the decoupling system interactions are thoughtful. Thus, a PI/PID must be implemented.

C. Decoupling Using Zlikind and Luyben Method

Using (11):

$$y = Gu^*,\ u^* = G_c^*u\,,\ u = G_c[w-y] \quad (24)$$

are chosen as follows:

$$y = GG_c^*u = GG_c^*G_c[w - y] \quad (25)$$

$$X = GG_c^* = \text{diag}[x_1, x_2]$$
$$G_c^*G^{-1}X\,, G^{-1} = \text{adj}(G)/\det(G) \quad (26)$$

where adj(G) is the adjoint of the matrix of G, and det(G) is the determinant of the matrix G given by:

$$\det(G) = G_{11}G_{22} - G_{12}G_{21} \quad (27)$$

$$\text{adj}(G) = \begin{bmatrix} G_{22} & -G_{12} \\ -G_{21} & G_{11} \end{bmatrix} \quad (28)$$

$$G_c^* = G^{-1}X \begin{bmatrix} G_{22}x_1 & G_{12}x_2 \\ G_{21}x_1 & G_{11}x_2 \end{bmatrix} \frac{1}{det(G)} \quad (29)$$

The chosen form is a unit diagonal given by:

$$G_{c,11}^* = G_{c,22}^* = 1 \quad (30)$$

therefore:

$$G_{c,12}^* = -\frac{G_{12}}{G_{11}}\,, \quad G_{c,21}^* = -\frac{G_{21}}{G_{22}} \quad (31)$$

G_{c1} and G_{c2} must be PI/PID regulators chosen as follows:

$$G_{c1} = G_{c2} = \frac{s+0.1}{s} \quad (32)$$

The Simulink transfer functions block wiring of this method is shown in Figure 8. Figure 9 shows the evolution of the outputs y1 and y2 applying the same conditions as in the other methods.

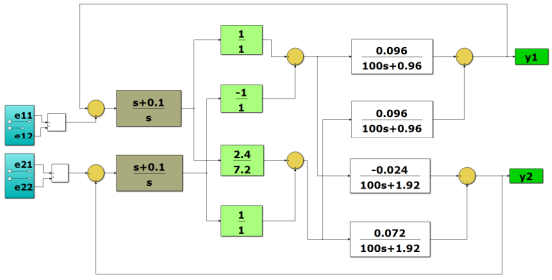

Fig. 8. Zlikind and Luyben Simulink block diagram.

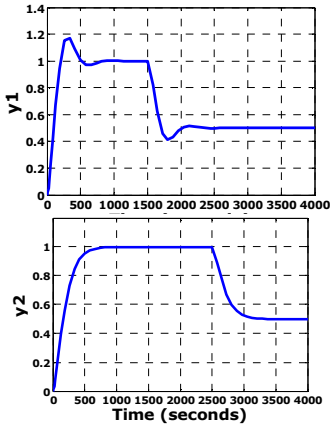

Fig. 9. Zlikind and Luyben grid outputs.

D. Decoupling Using Inverted Decoupling Method

G_{c11} and G_{c22} are placed in the forward direction which can be PI or PID controller. Using (11) and (12), it is necessary that:

$$D_{12} = -\frac{G_{12}}{G_{11}}\,, D_{21} = -\frac{G_{21}}{G_{22}} \quad (33)$$

The Simulink transfer wiring function wedges describing this method are shown in Figure 10.

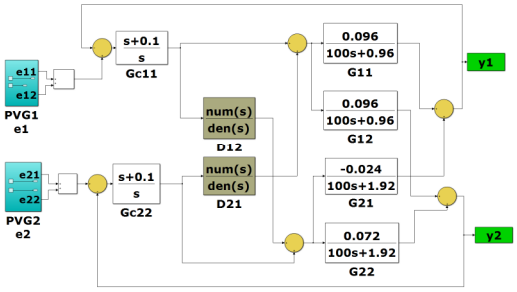

Fig. 10. Inverted decoupling block Simulink diagram.

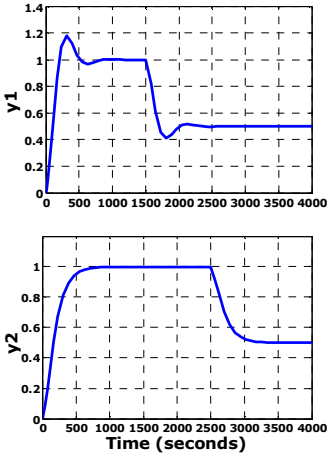

Fig. 11. Inverted decoupling grid outputs.

The inverted decoupling processes shown in Figure 11 does not contain bulk sums of transfer functions. Consequently, the diagonal controllers' fine-tuning becomes more accommodating in higher multivariable processes with solid cross-couplings, even if the system elements have simple changing aspects.

IV. RESULT COMPARISON AND DISCUSSION

The three methods obtained perfect decoupling, but the variation in the calculation of the terms that characterize each method and the simplicity of their use should be noted. In the Boksenbom and Hood method, the functions and the PI regulator were chosen in the decoupling block, but in the Zalkind and Luyben method they are taken equal to 1, which is simpler, and they do not appear based on a reduced decoupling block. The Zalkind and Luyben method requires the computation of the inverse $G(p)$, thus the determinant of G must be non-zero, which is not necessary for the two other

methods. The addition of a compensation block consisting of a PI controller in the direct chain for the Zalkind and Luyben decoupling method has the same effect as its addition in the decoupling block by the method based on the reduced decoupling block, so there is only a variation in the structure. Its absence in the Boksenbom and Hood method makes it lose flexibility in the implementation of the non-interactive control grouping, especially regarding the stability of the system. Using these criteria, the method based on a reduced decoupling block is the simplest because it requires fewer computations and has more flexibility via the PI controller.

A multivariable control system design employing a fine-tuning filter based on an inverted decoupler, using statue or output feedback control methods, was presented. The high closed-loop system enactment was attained for predefined robustness by eliminating unnecessary control exertion and introducing adequate filtration of the controlled variables. This was verified by the results which treat an extremely intermittent PV source and chain outputs. The proposed demand response path methods improved inverted decoupling. The disturbance response was minimized within a narrow range for the intermitting nature of renewable energy processes known for their instability.

V. CONCLUSION

The cogency of the proposed statue feedback multivariable control system design and tuning was confirmed using three methods. High closed-loop system performance was attained by avoiding unnecessary control exertion using the suitable controlled variables filtration. The three methods, Boksenbom and Hood, Zilkind and Luyben, and inverted decoupling, eliminated the opposing effects caused by non-minimum phase zeros and achieved dynamic decoupling.

The simulation results showed that the three proposed methods could establish a decent dynamic decoupling, solid robustness, and immunity against trouble. Results proved that they succeeded very effectively to limit the interactions of the inputs to the relative outputs, which opens the road to the generalization of these decoupling methods for the entire end-to-end chain of different energy sources to improve and optimize energy dispatching. Inverted decoupling gives more effective and precise results compared to Boksenbom and Hood and Zilkin and Luyben, given the additional regulation blocks G_{c11} and G_{c22}, which leads to maintaining the input magnitudes. Future work should assess more than two inputs and study a big-scale system matrix, rearranging it to a 2 by 2 matrix.

REFERENCES

[1] E. Gagnon, A. Pomerleau, and A. Desbiens, "Simplified, ideal or inverted decoupling?," *ISA Transactions*, vol. 37, no. 4, pp. 265–276, Sep. 1998, https://doi.org/10.1016/S0019-0578(98)00023-8.

[2] P. Chen and W. Zhang, "Improvement on an inverted decoupling technique for a class of stable linear multivariable processes," *ISA Transactions*, vol. 46, no. 2, pp. 199–210, Apr. 2007, https://doi.org/10.1016/j.isatra.2006.09.002.

[3] B. T. Jevtović and M. R. Mataušek, "PID controller design of TITO system based on ideal decoupler," *Journal of Process Control*, vol. 20, no. 7, pp. 869–876, Aug. 2010, https://doi.org/10.1016/j.jprocont.2010.05.006.

[4] J. Garrido, F. Vázquez, and F. Morilla, "An extended approach of inverted decoupling," *Journal of Process Control*, vol. 21, no. 1, pp. 55–68, Jan. 2011, https://doi.org/10.1016/j.jprocont.2010.10.004.

[5] H. Wang, Y. Zhu, and J. Chen, "A design method of decoupling IMC controller for multi-variable system based on Butterworth filter," in *2017 American Control Conference (ACC)*, Seattle, WA, USA, Feb. 2017, pp. 5714–5719, https://doi.org/10.23919/ACC.2017.7963845.

[6] S. Li, M. Luan, D. Gan, and D. Wu, "A model-based decoupling observer to locate forced oscillation sources in mechanical power," *International Journal of Electrical Power & Energy Systems*, vol. 103, pp. 127–135, Dec. 2018, https://doi.org/10.1016/j.ijepes.2018.05.014.

[7] S. A. C. Giraldo, R. C. C. Flesch, J. E. Normey-Rico, and M. Z. P. Sejas, "A Method for Designing Decoupled Filtered Smith Predictor for Square MIMO Systems With Multiple Time Delays," *IEEE Transactions on Industry Applications*, vol. 54, no. 6, pp. 6439–6449, Aug. 2018, https://doi.org/10.1109/TIA.2018.2849365.

[8] A. Trejos, D. Gonzalez, and C. A. Ramos-Paja, "Modeling of Step-up Grid-Connected Photovoltaic Systems for Control Purposes," *Energies*, vol. 5, no. 6, pp. 1900–1926, Jun. 2012, https://doi.org/10.3390/en5061900.

[9] A. Vijayakumari, A. T. Devarajan, and N. Devarajan, "Decoupled control of grid connected inverter with dynamic online grid impedance measurements for micro grid applications," *International Journal of Electrical Power & Energy Systems*, vol. 68, pp. 1–14, Jun. 2015, https://doi.org/10.1016/j.ijepes.2014.12.015.

[10] M. Ashabani, Y. A.-R. I. Mohamed, M. Mirsalim, and M. Aghashabani, "Multivariable Droop Control of Synchronous Current Converters in Weak Grids/Microgrids With Decoupled dq-Axes Currents," *IEEE Transactions on Smart Grid*, vol. 6, no. 4, pp. 1610–1620, Jul. 2015, https://doi.org/10.1109/TSG.2015.2392373.

[11] I. Rahimi Pordanjani and W. Xu, "A singular value decomposition-based technique for decoupling and analyzing power networks," *International Journal of Electrical Power & Energy Systems*, vol. 74, pp. 265–273, Jan. 2016, https://doi.org/10.1016/j.ijepes.2015.07.028.

[12] Y. Zhang, M. G. L. Roes, M. A. M. Hendrix, and J. L. Duarte, "Symmetric-component decoupled control of grid-connected inverters for voltage unbalance correction and harmonic compensation," *International Journal of Electrical Power & Energy Systems*, vol. 115, Feb. 2020, Art. no. 105490, https://doi.org/10.1016/j.ijepes.2019.105490.

[13] S. Li, Y. Li, X. Chen, W. Jiang, X. Li, and T. Li, "Control strategies of grid-connection and operation based on active disturbance rejection control for virtual synchronous generator," *International Journal of Electrical Power & Energy Systems*, vol. 123, Dec. 2020, Art. no. 106144, https://doi.org/10.1016/j.ijepes.2020.106144.

[14] A. A. Nazari, R. Keypour, M. H. Beiranvand, and N. Amjady, "A decoupled extended power flow analysis based on Newton-Raphson method for islanded microgrids," *International Journal of Electrical Power & Energy Systems*, vol. 117, May 2020, Art. no. 105705, https://doi.org/10.1016/j.ijepes.2019.105705.

[15] C. Zhao, J. Xia, C. Guo, and R. Zhan, "An improved control strategy for current source converter-based HVDC using fundamental frequency modulation," *International Journal of Electrical Power & Energy Systems*, vol. 133, Dec. 2021, Art. no. 107265, https://doi.org/10.1016/j.ijepes.2021.107265.

[16] B. Liu *et al.*, "Integration of power decoupling buffer and grid-tied photovoltaic inverter with single-inductor dual-buck topology and single-loop direct input current ripple control method," *International Journal of Electrical Power & Energy Systems*, vol. 125, Feb. 2021, Art. no. 106423, https://doi.org/10.1016/j.ijepes.2020.106423.

[17] D. Khan, M. Khan, Y. Ali, A. Ali, and I. Hussain, "Resonance Mitigation and Performance Improvement in Distributed Generation based LCL Filtered Grid Connected Inverters," *International Journal of Advanced Computer Science and Applications*, vol. 10, no. 12, pp. 55-63, Jan. 2019, https://doi.org/10.14569/IJACSA.2019.0101208.

[18] S. B. A. Kashem, M. E., A. Khandakar, J. Ahmed, A. Ashraf, and N. Shabrin, "Wind Power Integration with Smart Grid and Storage System: Prospects and Limitations," *International Journal of Advanced*

Computer Science and Applications, vol. 11, no. 5, pp. 552–569, 2020, https://doi.org/10.14569/IJACSA.2020.0110570.

[19] M. Z. Khan, M. Mansoor, X. Xiangming, U. Khalid, and M. Ahmed, "An Optimal Control Load Demand Sharing Strategy for Multi-Feeders in Islanded Microgrid," *International Journal of Advanced Computer Science and Applications*, vol. 9, no. 12, pp. 18–25, 2018, https://doi.org/10.14569/IJACSA.2018.091203.

[20] S. Younsi and N. Hamrouni, "Control of Grid Connected Three-Phase Inverter for Hybrid Renewable Systems using Sliding Mode Controller," *International Journal of Advanced Computer Science and Applications*, vol. 9, no. 11, pp. 336–343, 2018, https://doi.org/10.14569/IJACSA. 2018.091146.

[21] R. Abbassi, "SOGI-based Flexible Grid Connection of PV Power Three Phase Converters under Non-ideal Grid Conditions," *Engineering, Technology & Applied Science Research*, vol. 10, no. 1, pp. 5195–5200, Feb. 2020, https://doi.org/10.48084/etasr.3263.

[22] A. Elgharbi, D. Mezghani, and A. Mami, "Intelligent Control of a Photovoltaic Pumping System," *Engineering, Technology & Applied Science Research*, vol. 9, no. 5, pp. 4689–4694, Oct. 2019, https://doi.org/10.48084/etasr.2982.

[23] M. Y. Allani, D. Mezghani, F. Tadeo, and A. Mami, "FPGA Implementation of a Robust MPPT of a Photovoltaic System Using a Fuzzy Logic Controller Based on Incremental and Conductance Algorithm," *Engineering, Technology & Applied Science Research*, vol. 9, no. 4, pp. 4322–4328, Aug. 2019, https://doi.org/10.48084/etasr.2771.

[24] S. Javadpoor and D. Nazarpour, "Modeling a PV-FC-Hydrogen Hybrid Power Generation System," *Engineering, Technology & Applied Science Research*, vol. 7, no. 2, pp. 1455–1459, Apr. 2017, https://doi.org/ 10.48084/etasr.760.

AUTHORS PROFILE

Salim Nebili was born in Gafsa, Tunisia, in 1973. He received the Engineering Degree from the National Engineering School of Gabes (ENIG) in 1998 and a Master's degree in 2002 from the National Engineering School of Tunis (ENIT). He is a member of the Analysis and Treatment of Electrical and Energetic Signals and Systems Laboratory. His research interests include electrical engineering, renewable energies, and smart grids.

Ibrahim Benabdallah was born in Tunis, Tunisia, in 1984. He received a Master's and Doctor's degree in Electronics from the Faculty of Sciences of Tunis (FST). He is a member of the Analysis and Treatment of Electrical and Energetic Signals and Systems Laboratory. His research interests include electrical engineering, renewable energies, and smart grids.

Adnen Cherif received Engineer, Master, and PhD degrees from the National Engineering School (ENIT) of Tunis, Tunisia. Since 1997, he is a senior professor and responsible for the Analysis and Treatment of Electrical and Energetic Signals and Systems (ATEESS) Laboratory in the Faculty of Science of Tunis, Tunisia. His fields of interest concern digital signal processing, speech processing, energetic systems, renewable energies, and smart grids.